Linear and nonlinear compact modes in quasi-one-dimensional flatband systems

Dany López-González and Mario I. Molina
Department of Physics, MSI-Nucleus on Advanced Optics, and Center for Optics and Photonics (CEFOP), Faculty of Sciences, University of Chile, Santiago, Chile
(Received 21 January 2016; published 26 April 2016)

We examine analytically and numerically the spectral properties of three quasi-one-dimensional lattices, namely, kagome, Lieb, and stub lattices, which are characterized for having flatbands in their spectrum. It is observed that the degenerate eigenmodes modes of these flatbands form a Starklike ladder where each mode is shifted by one lattice site. Their combination can give rise to compact modes that do not diffract due to a geometrical phase cancellation. For all three cases we computed the stability of the fundamental band mode against perturbation of their amplitude and phase, the effect of possible anisotropy of the couplings, and the presence of small random perturbations of the coupling. For the Lieb and stub ribbon, the compact mode turns out to be quite robust and the flatband survives, while for the kagome ribbon, the compact mode is destroyed and the flatband is lost. When adding nonlinear effects, the compact mode turns out to be also a nonlinear eigenvector, with a power curve that is proportional to the eigenvalue and exists for any eigenvalue, in marked contrast to the usual case of discrete solitons, which can exist only outside the linear bands. These properties look promising for a future design of a robust system for long-distance propagation of information.

DOI: 10.1103/PhysRevA.93.043847

I. INTRODUCTION

The problem of localization of excitations in periodic systems is a topic that has maintained interest throughout the years [1]. In general, the available mechanisms for achieving a degree of localization had to rely on nonlinear effects, via self-trapping, or on a breaking of the translational symmetry of the lattice via, e.g., the presence of impurities, extended defects, or a completely disordered medium. In the last case, complete localization is achieved in one- and two-dimensional lattices, termed Anderson localization.

Recently, however, another mechanism for achieving localization has gained increasing interest: flatbands. A flatband lattice is a periodic system characterized by having one or more flatbands in its spectrum. Since the group velocity of a state belonging to one of these bands is zero, any flatband eigenstate or a superposition of them will exhibit no mobility. Some systems where flatbands have been studied and observed include optical [2,3] and photonic lattices [4–6], graphene [7,8], superconductors [9–12], fractional quantum Hall systems [13–15], and exciton-polariton condensates [16,17]. The presence of a flatband in the spectrum of a hermitian lattice implies the existence of a set of entirely degenerate states, whose superposition displays no dynamical evolution. This allows the formation of compacton-like structures, which are completely localized in space, constituting a new form of localized state in the continuum [18]. The origin of these compact states rely on a precise geometrical interference condition. Such states have been recently observed experimentally in an optical waveguide array forming a Lieb lattice in the transversal direction [5,6]. This raises the possibility that a judicious superposition of these compacton-like states can be used to generate a whole set of diffraction-free modes that can carry information for long distances in an optical waveguide array. Since there are no flatbands for pure one-dimensional lattices, it becomes interesting to explore them in quasi-one-dimensional periodic systems, i.e., ribbons. Such lattices could be easily fabricated using the femtosecond laser-writing technique [19,20] and are more economical than a full-blown two-dimensional lattice.

In this work we study analytically and numerically the spectrum and localization properties of three quasi-one-dimensional optical lattices which possess flatbands, namely, Lieb, kagome, and stub lattices, and how their spectra is affected by the presence of perturbations that break the delicate geometrical interference needed for a flatband to exist. This is important in order to assess the real usefulness of flatband systems as possible candidates for stable long-distance image transmission systems.

II. THE MODEL

Let us consider a quasi-one-dimensional lattice (ribbon) representing, for example, a cross section of a nonlinear (Kerr) optical waveguide array (Fig. 1). In this context and in the coupled-modes framework, the evolution of the electric field on guide $\mathbf{n}$ is given by [21]

$$i\frac{d}{dz}C_{\mathbf{n}}(z)+\sum_{\mathbf{m}}V_{\mathbf{m},\mathbf{n}}C_{\mathbf{m}}(z)+\gamma|C_n(z)|^2C_n(z)=0, \qquad (1)$$

where $C_{\mathbf{n}}(z)$ is proportional to the amplitude of the electric field at site $\mathbf{n}$, z is the propagation coordinate (measured in meters), and $V_{\mathbf{m},\mathbf{n}}$ is the coupling among waveguides (measured in 1/meter), and the sum in Eq. (1) is restricted to nearest-neighbor sites only. Parameter γ is the nonlinear coefficient (in units of 1/watt$\times$ meter), and in this case $\gamma=\omega_0 n_2/cA_{\text{eff}}$, where ω_0 is the angular frequency of the light, n_2 is the nonlinear coefficient of the guides, and A_{eff} is the effective area of the linear modes.

Stationary modes are obtained from the ansatz $C_{\mathbf{n}}(z)=C_{\mathbf{n}}\exp(i\Omega z)$, where the $C_{\mathbf{n}}$ amplitudes obey

$$-\Omega C_{\mathbf{n}}+V\sum_{\mathbf{m}}C_{\mathbf{m}}+\gamma|C_{\mathbf{n}}|^2C_{\mathbf{n}}=0, \qquad (2)$$

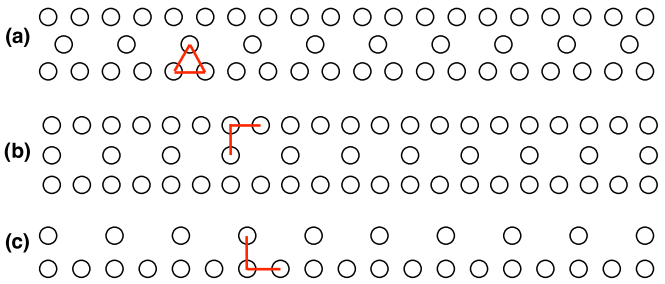

FIG. 1. Quasi-one-dimensional arrays. (a) Kagome ribbon, (b) Lieb ribbon, (c) Stub ribbon. The lines between dots connect nearest neighbor sites.

where Ω is the propagation constant of the mode. System (2) represents a system of coupled nonlinear equations, whose solutions can be found numerically by using a multidimensional Newton-Raphson method, where one uses the weakly coupled limit (high nonlinearity) as the initial condition. The families of nonlinear solutions thus found are classified by the power content of the mode, $P = \sum_{\mathbf{n}} |C_{\mathbf{n}}|^2$, and its propagation constant Ω. It should be mentioned that P is also a constant of motion.

The linear stability of these nonlinear modes can be computed as follows [22]: We introduce a weak perturbation as $C_n(z) = [C_n + u_n(z) + i\,v_n(z)]\exp(i\Omega z)$ and obtain linear evolution equations for the real functions u_n and v_n that we can express in compact form by defining real vectors $\delta\mathbf{U}\{u_n\}$ and $\delta\mathbf{V}\{v_n\}$. With these definitions the combined linear equations can be written in the form $\delta\ddot{\mathbf{U}} + \mathbf{BA}\,\delta\,\mathbf{U} = 0$ and $\delta\ddot{\mathbf{V}} + \mathbf{AB}\,\delta\mathbf{V} = 0$, where the overdots stand for the derivative in z. Therefore, the linear stability of nonlinear localized modes is defined by the eigenvalue spectra of the matrices **AB** and **BA** (they have same eigenvalues). If any of the real eigenvalues is negative, the corresponding nonlinear stationary solution is unstable; otherwise, the solution is stable. Let $\{\omega^2\}$ be the eigenvalue spectra of **AB** or **BA**, then we define the instability gain as the largest imaginary part of the eigenvalues, $g = \max\{|\mathrm{Im}[\omega^2]|\}$. Thus, a given solution is stable when $g = 0$; otherwise it is unstable.

A. The kagome ribbon

1. Linear regime

The thinnest kagome ribbon is shown at the top of Fig. 1. This geometry has been used in the past in studies of magnetization in frustrated quantum lattices [23]. This ribbon has five sites in its unit cell, which implies five bands, given by

$$\begin{aligned}\Omega &= -2\,V,\\ \Omega &= \pm\sqrt{2[1+\cos(2k)]}\;V,\\ \Omega &= [1 \pm \sqrt{3+2\cos(2k)}]\;V.\end{aligned} \tag{3}$$

Thus, we have the flatband $\Omega = -2V$. In Fig. 2 we show all five bands.

2. Stationary modes

At the top of Fig. 3 we plot the eigenvalues of the whole system in order of increasing value. The flatband at $\Omega = -2V$ is clearly visible. We look now for the modes belonging to the five bands. For $\gamma = 0$ we solve linear equations (2) and obtain all the linear modes of the ribbon. We then plot them as a function of site number by "hanging" them in order of increasing eigenvalue. The result is shown in the bottom panel of Fig. 3, whose complexity is only apparent. The plot appears divided into sectors because of the particular numbering employed for the sites. For a total number of $N = 150$ sites,

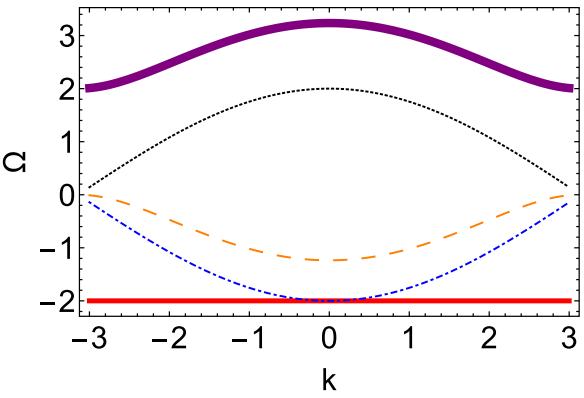

FIG. 2. The five bands of the kagome ribbon, $V = 1$.

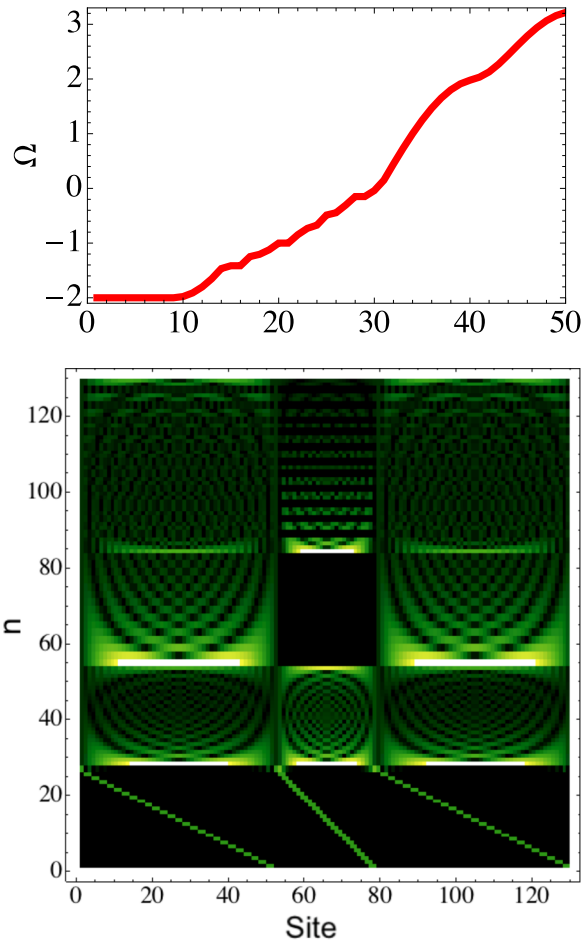

FIG. 3. Top: Eigenvalues of the kagome ribbon, arranged in order of increasing value. The flatband is clearly appreciable at $\Omega = -2V$. Bottom: Density plot of the eigenvectors of the kagome ribbon, arranged in order of increasing eigenvalue ($N = 150$).

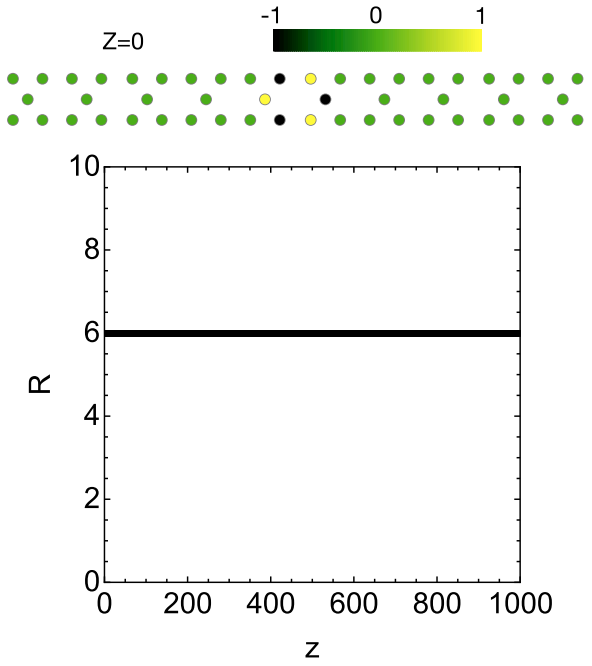

FIG. 4. Top: Fundamental compact ring mode belonging to the flatband. Every site on the ring possesses equal amplitude, but their phases change by π when moving from site to site along the ring. Bottom: Participation ratio R of the ring mode as a function of the evolution coordinate z.

the first 22 lowest eigenvectors (belonging to the degenerate eigenvalue $\Omega = -2V$), we see that the modes are quite localized and form a Starklike ladder with each mode being shifted by one lattice site. The rest of the modes belonging to the dispersive bands show extended states as usual. It should be noticed that these Starklike modes really occupy a band of zero width, since they all have the same eigenvalue. The bandlike distributions are an artifact of the plot.

Since the modes of the flatband are very localized, they can be combined to give rise to a set of compact-like modes, like the one shown in Fig. 4. It is straightforward [from (2)] to show that this ring mode is indeed a stationary mode of the flatband. Along the ring, there is a π phase difference between sites, which leads to a phase cancellation on nearby sites, producing in this manner absence of transversal diffraction. The spatial extension of a mode can be computed from the participation ratio $R = (\sum_i |C_i|^2)^2 / \sum_i |C_i|^4$. For a completely localized mode, $R = 1$, while for a delocalized mode $R = N$. This parameter gives an idea of the sites that are effectively excited during the dynamical evolution. Figure 4 also shows R for the ring mode as it evolves with z, and we see clearly that the mode remains perfectly compact for long evolution distances.

The existence of a flatband populated with compact, diffractionless modes implies also the existence of linear dynamical self-trapping: If we take a single excited site as an initial condition and examine its evolution, one will notice that while most of the amplitude propagates away from the initial site, a fraction will remain trapped at the initial site asymptotically. The reason for this is that the initial localized excitation is a superposition of all modes of the bands, including states from the flatband. During evolution, the contributions from the dispersive bands will diffract away while the portion coming from the flatband will remain in place, giving rise to partial self-trapping. This particular mode of self-trapping has been observed before [24]. It should be mentioned that larger rings, or judicious combinations of small rings, can also give rise to diffractionless modes (not shown). The only requisite is the geometrical phase cancellation. A large number of compact modes can be thus generated in this way.

3. *Dynamical stability*

We begin our stability study by examining the robustness of the kagome flatband against perturbations or errors in the initial state of the fundamental ring shown in Fig. 4. Thus, we define the initial state of the ring as $C_j = A_j + \delta A_j$, where $\delta A_j \in [-w, w]$, where w is the width of the noise. Around the ring the amplitudes A_j have the same absolute value but alternate in sign. Outside the ring, $C_j = 0$. In an optical setting, this is equivalent to altering the refraction index of the wave guides, which can be done by controlling the writing speed of the guides that are created with the laser-writing technique[19,20]. Figure 5 shows the evolution of the participation ratio of the ring mode at long propagation distances, for several noise strengths. Clearly, the ring is robust against this kind of perturbation.

Let us now investigate the effect of anisotropic couplings. We define the anisotropy parameter $\delta = V_h / V_d$ where V_d corresponds to the coupling between nearest neighbors along the diagonal direction, and V_h corresponds to the coupling between nearest neighbors along the horizontal direction [see Fig. 1(a)].

A quick numerical inspection of all the eigenvalues reveals that, as soon as the anisotropy parameter is different from zero, the flatband is lost (Fig. 6). The participation ratio seems to reach a high, constant value, but this is an artifact due to the finite length of the ribbon, where the wave is reflected by the ribbon boundaries.

The values of the participation ratio R as it evolves in z are shown in Fig. 7 and confirm that the flatbands are destroyed as soon as the anisotropy parameter is different from unity. Even for small anisotropies R differs substantially from the expected value of 6.

What this means is that it will be hard to experimentally observe the flatbands in an optical setting, since the current technology to produce the waveguide arrays is based on the femtosecond laser-writing technique[19,20], which tends to produce guides with high ellipticity and, thus, anisotropic couplings.

Finally, let us study the inclusion of noise in the couplings: $V \to V + \delta V$, with $\delta V \in [-w, w]$. Figure 8 shows the eigenvalues and the participation ratio for different w values. We can see that the flatband is destroyed, and the participation ratio changes rapidly away from the initial value of six. The oscillations in R are due to Anderson localization that produces a localized profile with fluctuating boundaries.

4. *Nonlinear regime*

Here we examine the nonlinear properties of the kagome ribbon focusing on some simple representative nonlinear modes. Now we take $\gamma \neq 0$ in Eq. (2). We begin by looking

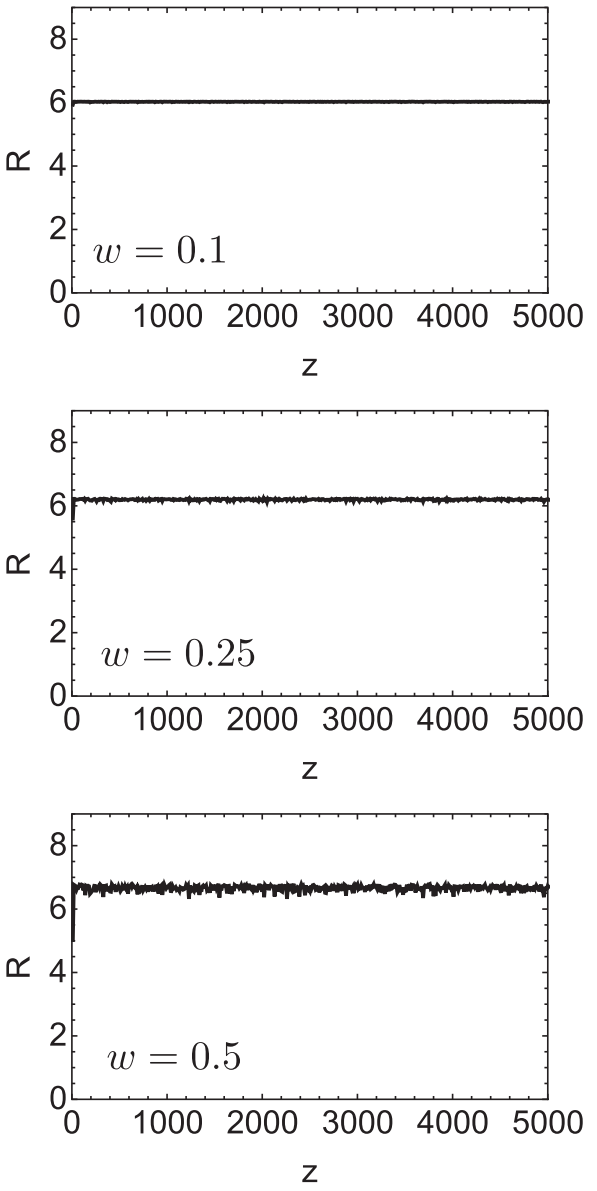

FIG. 5. Participation ratio R of the fundamental ring as a function of z for a random perturbation of the initial conditions. The width of the noise is $w = 0.1$ (top), $w = 0.5$ (middle), and $w = 1.0$ (bottom).

for modes that exist outside of the bands and located around a single site. For $\gamma > 0$ we are above the band maximum $\Omega = V[1 + \sqrt{2 + \cos(\pi)}] \sim 3.2$, while for $\gamma < 0$ we are below the band minimum $\Omega = -2V$. In the anticontinuum limit and for modes centered around a single site, we will examine two different initial sites (see inset in Figs. 9 and 11).

Figure 9 shows the power versus propagation constant curve, for a nonlinear mode centered on an edge site. The curve resembles the one for a two-dimensional lattice. We observe a minimum power value for the mode (also termed a discrete soliton) to exist. To the left of this critical value the mode is linearly unstable. In Fig. 10 we show the participation ratio of this mode as a function of its power content and its instability gain as a function of the mode propagation constant. We see that in the unstable regime the mode tends to expand, while in the other branch it tends to decrease, signaling a tendency to

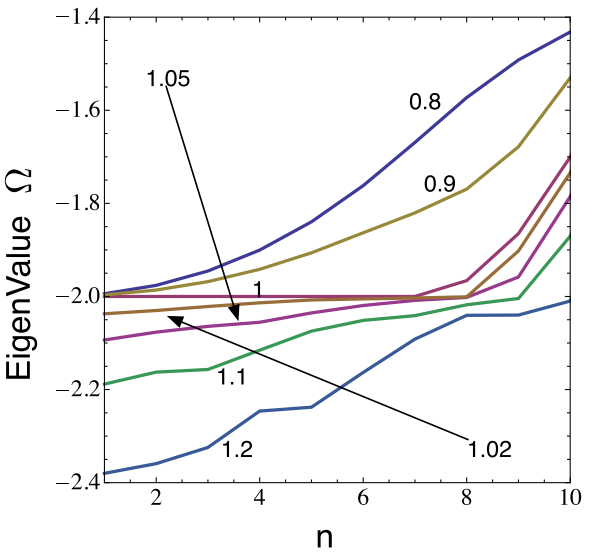

FIG. 6. Eigenvalues Ω for a large ($N = 120$) kagome ribbon for different values of the anisotropy parameter δ. The eigenvalues are plotted in order of increasing value and just the flatband region is shown.

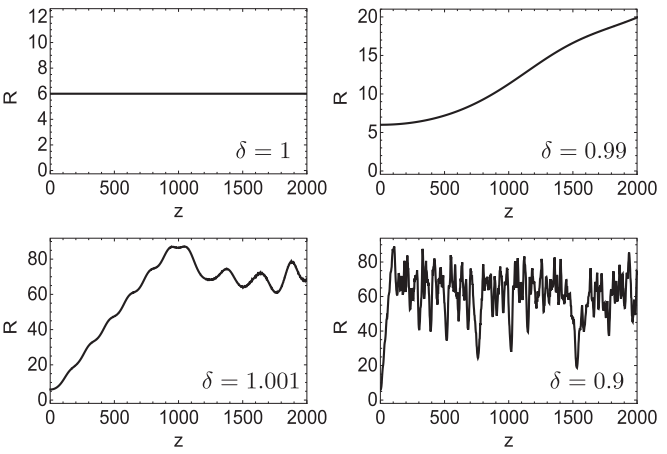

FIG. 7. Kagome ribbon. Evolution of the participation ratio R for different values of the anisotropy parameter δ in the couplings.

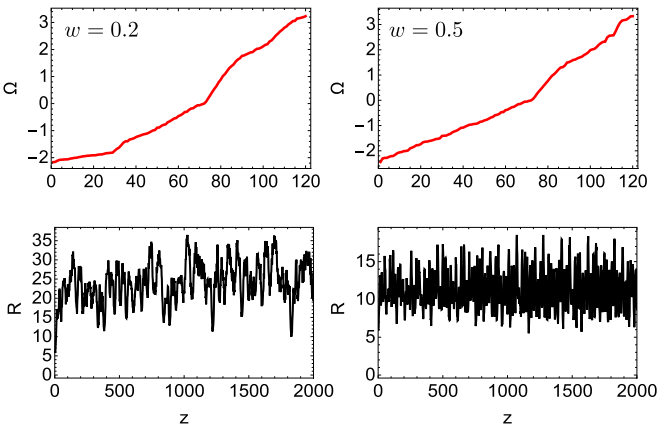

FIG. 8. Kagome ribbon with coupling disorder. Top: Eigenvalues of the kagome ribbon, ordered according to increasing value. Bottom: Evolution of the participation ratio of the compact mode, for different disorder widths.

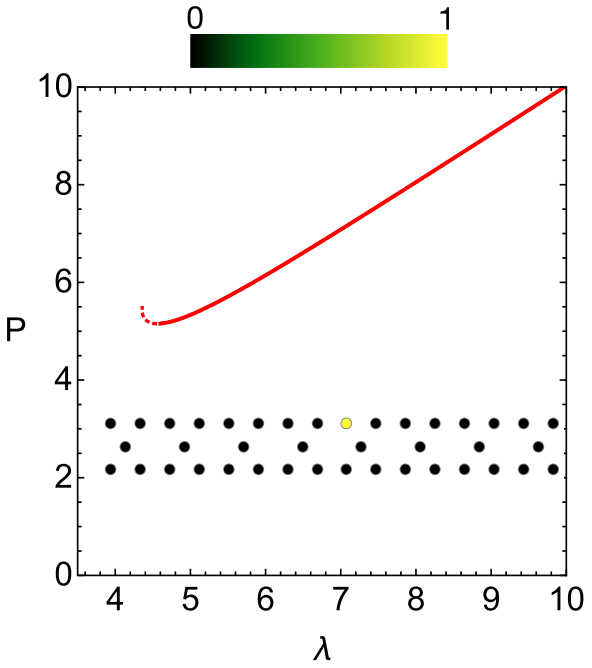

FIG. 9. Power vs propagation constant diagram for the fundamental compact kagome mode. Continuous (dashed) line denotes stable (unstable) behavior.

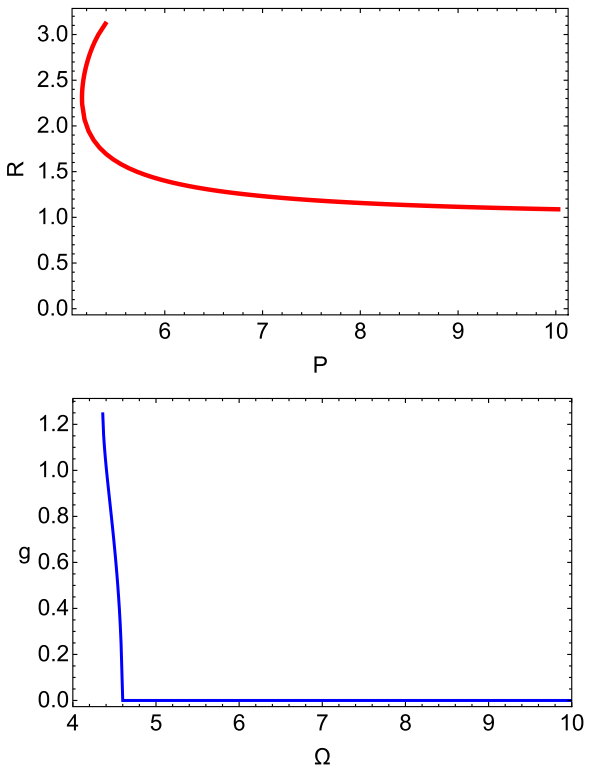

FIG. 10. Kagome ribbon. Top: Participation ratio as a function of the power content of the nonlinear mode depicted in Fig. 9. Bottom: Stability gain vs the nonlinear mode propagation constant. The onset of instability is clearly visible around $\Omega \sim 4.6$.

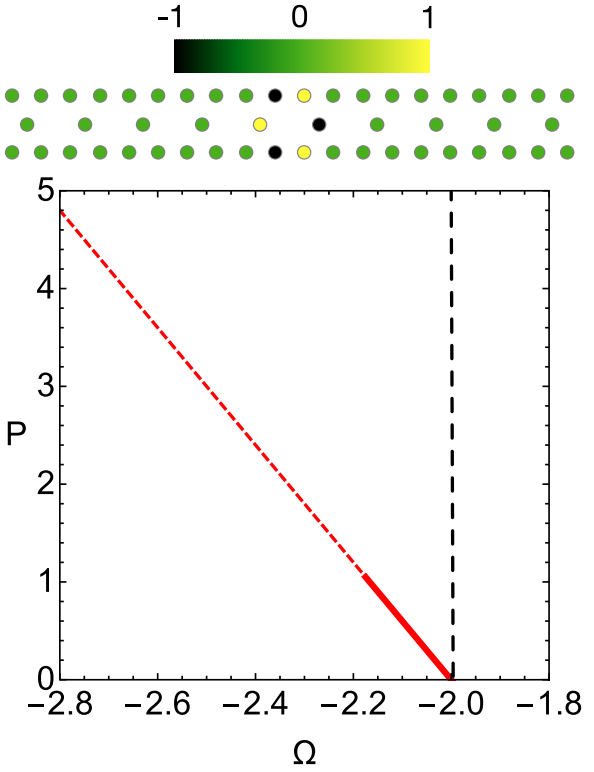

FIG. 11. Kagome ribbon. Power vs propagation constant diagram for the fundamental compact kagome mode. Continuous (dashed) line denotes stable (unstable) behavior.

localization. Also the instability gain tends to increase rapidly, the closer we are to the outermost band edge. In the case of a nonlinear mode centered on an "inner site" of the ribbon, the power versus propagation constant is different from its previous "surface" counterpart. Now, the power curve (not shown) reaches all the way to the edge of the band, and it is stable everywhere. The shape of the curve resembles the one found in pure one-dimensional chains.

What about the compact kagome ring mode? It turns out that this mode is also an eigenmode of the linear system. From Eq. (2), one obtains the power curve in closed form

$$P = \frac{6}{\gamma}(\Omega + 2V), \tag{4}$$

and, thus, it does not require a minimum power to exist. Its stability diagram, shown in Fig. 11, shows the existence of a critical power ($P \sim 1.1$) above which the mode becomes unstable, although its computed participation ratio remains at a value of six, indicating that this mode does not lose its ring shape.

B. The Lieb ribbon

1. Linear regime

The Lieb ribbon is shown in Fig. 1(b). It consists essentially of a depleted square lattice ribbon. Its unitary cell contains five units, which implies five bands:

$$\begin{aligned} &\Omega = 0, \\ &\Omega = \pm\sqrt{2[1+\cos(2k)]}V, \\ &\Omega = \pm\sqrt{4+2\cos(2k)}V. \end{aligned} \tag{5}$$

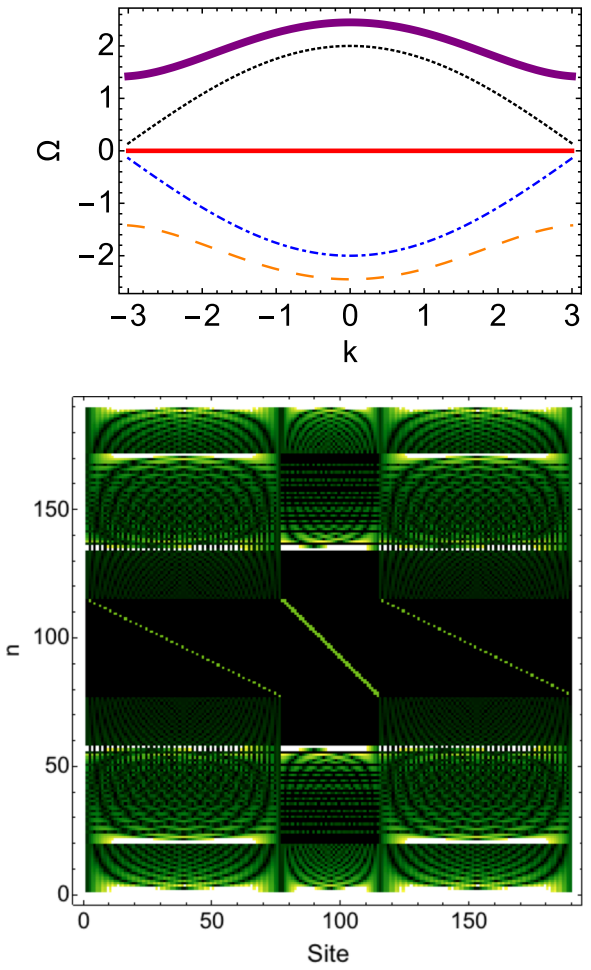

FIG. 12. Top: The five bands of the Lieb ribbon. Bottom: Density plot of the eigenvectors of the Lieb ribbon, arranged in order of increasing eigenvalue.

Thus, as Fig. 12 (top) shows, out of the five bands, we have the flatband $\Omega = 0$. The modes belonging to this band have zero group velocity, which leads to a sharp transverse localization. These compacton-like modes are able to propagate along the guide without diffraction. As mentioned earlier, the reason for this localization is a geometric phase cancellation among nearby sites. Also, as in the kagome ribbon, one can have larger ring structures, or a judicious combination of small rings, and create other diffractionless modes (not shown).

2. *Stationary modes*

As was done for the kagome lattice, we set $\gamma = 0$ and solve the linear equation (2). Next we "hang" the eigenvectors in order of increasing eigenvalue, generating the density plot shown at the bottom of Fig. 12. Again, we note that for eigenvalue $\Omega = 0$, the degenerate eigenstates form a Stark ladder, while all the other modes belonging to the dispersive bands are extended. As was mentioned before, all of these Starklike modes really occupy a band of zero width, since they all have the same eigenvalue. The bandlike distribution is an artifact of the plot.

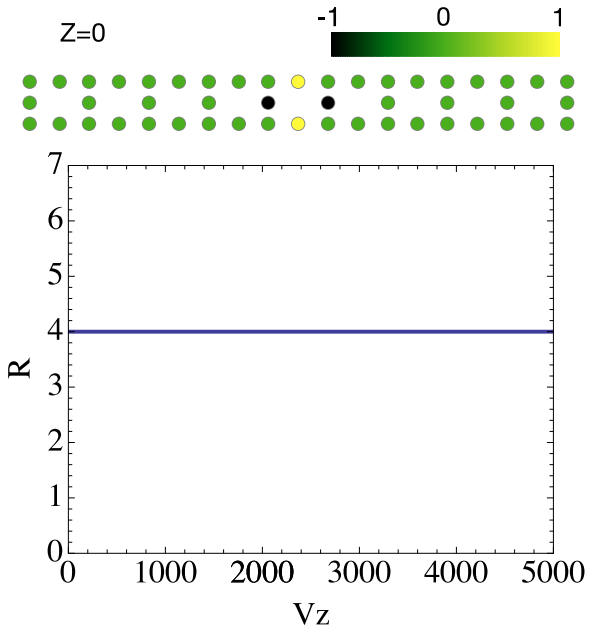

FIG. 13. Evolution of the participation ratio of the fundamental compact ring of the Lieb ribbon.

As in the kagome ribbon, the Lieb system has an compact eigenstate in the form of a square ring, which can evolve for long times without experiencing any diffraction (Fig. 13).

As we did for the Kagome case, let us also perturb this square compact ring, by introducing small random errors to the value of the ring amplitudes, $A_j \to A_j + \delta A_j$ where $\delta A_j \in [-w, w]$. The evolution of the participation ratio of the ring mode (not shown) shows that R is constant for all distances, even for large δ values. This is also observed for the kagome ribbon (Fig. 5).

Let us now investigate the effect of (nonrandom) anisotropic couplings. We define the anisotropy parameter $\delta = V_h/V_v$ where V_v corresponds to the coupling between nearest neighbors along the vertical direction, and V_h corresponds to the coupling between nearest neighbors along the horizontal direction [see horizontal and vertical lines in Fig. 1(b)]. At the top of Fig. 14 we show the eigenvalues and the participation ratio obtained for two different values of the anisotropy parameter $\delta = V_h/V_v$. As we can see, the flatband persists for these two δ values, even for $\delta \gg 1$. The dispersive bands show the onset of energy gaps for certain large δ values. For small δ values R remain pinned to its value of 4, while for larger δ it shows some oscillations around 4. The source of these oscillations seem to originate from an amplitude transfer among the four sites that occurs at high δ and is visible in the insets.

Finally, let us complete the dynamical stability analysis, by examining the effect of random perturbations of the couplings, $V \to V + \delta V$, where $\delta V \in [-w, w]$, in the absence of anisotropy. As can be seen in the bottom panels of Fig. 14, the existence of noise in the couplings does not destroy the flatband and only introduces some oscillations in the participation ratio, coming from irregular amplitude transfer among the four sites of the fundamental ring. The situation is rather similar to the case of anisotropic couplings.

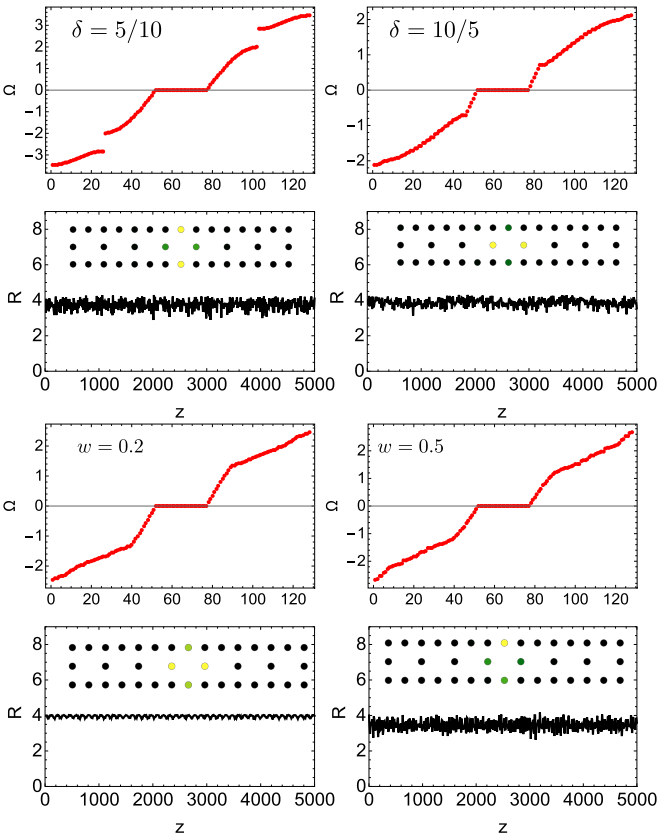

FIG. 14. The first four upper plots show the eigenvalue (Ω) and the participation ratio of the Lieb ribbon for two different anisotropies δ and zero disorder ($w = 0$), while the lower four plots show Ω and R for two different disorder widths w and zero anisotropy ($\delta = 0$).

3. *Nonlinear regime*

As in the previous kagome case, the fundamental Lieb mode, composed of four sites, is also a nonlinear mode of Eq. (2). It is straightforward to obtain the power curve for this mode:

$$P = \frac{4}{\gamma}\frac{\Omega}{V}. \tag{6}$$

From the numerical stability analysis (Fig. 15), we obtain that the mode is unstable at low powers up to a critical Ω value, beyond which it becomes stable.

By computing the participation ratio as a function of the power, we observe (not shown here) that the shape of the square ring does not change throughout the increase in power.

Now, let us consider a mode centered on a single site in the middle of the ribbon. As we can see in Fig. 16, the power versus propagation constant shows a region of bistability, where two stable regimes are separated by an unstable one. The stable power curve extends all the way to zero power, where the mode reaches the exterior edge of the bands. In this case, the mode ceases to exists as soon as it reaches the bands, in marked contrast to the square ring mode, which exists for any amount of power and any value of the propagation constant.

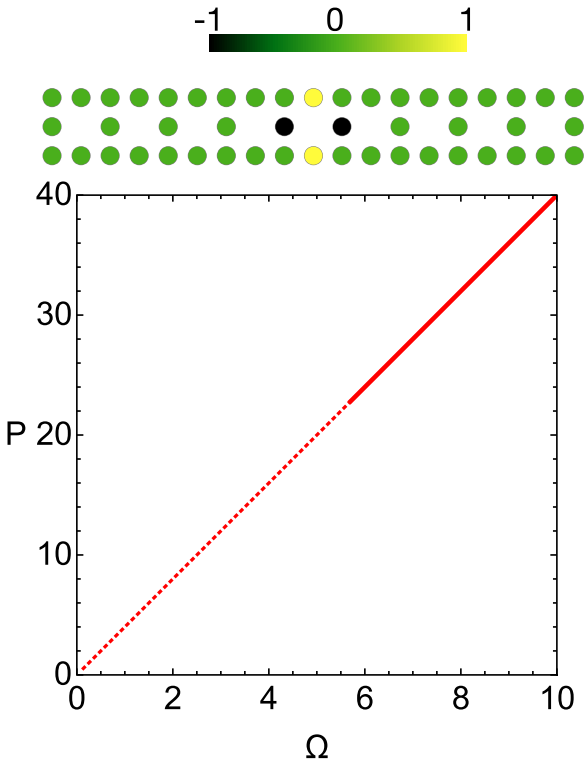

FIG. 15. Power vs propagation constant diagram for the fundamental compact Lieb mode. Continuous (dashed) line denotes stable (unstable) behavior.

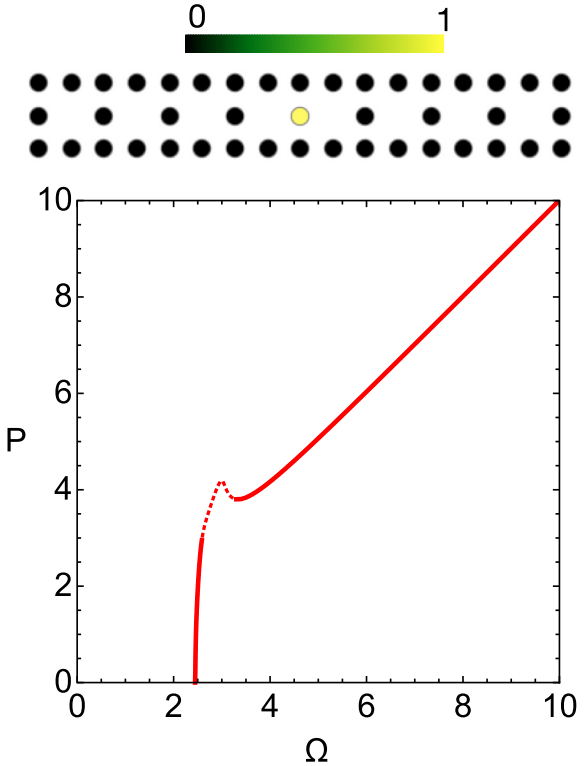

FIG. 16. Power vs propagation constant diagram for a mode centered on a single site in the middle of the Lieb ribbon. Continuous (dashed) line denote stable (unstable) behavior.

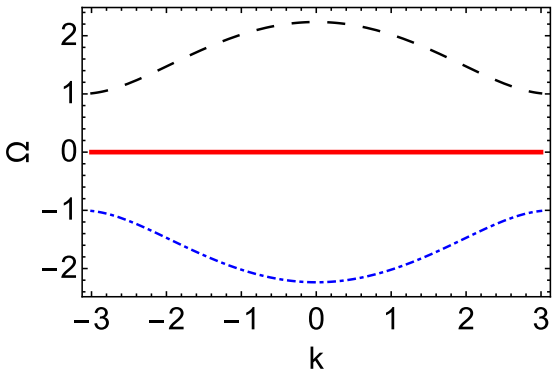

FIG. 17. The three bands of the stub ribbon.

4. The stub ribbon

The stub ribbon is shown at the bottom row of Fig. 1. Its geometry has been used in the past in studies on boson and fermion dynamics [3]. Its unitary cell has three sites, leading to three real bands:

$$\Omega = 0,$$
$$\Omega = \pm\sqrt{3 + 2\cos(2k)}\, V, \tag{7}$$

where, as in the Lieb case, we have a flatband at $\Omega = 0$. Figure 17 shows the shape of the three bands

5. Linear regime

As we observed for the kagome and Lieb ribbon, we see that for $\Omega = 0$, the degenerate eigenstates form a Stark ladder, while all the other modes belonging to the dispersive bands are extended (Fig. 18). Again we note that the band of these Stark modes is of zero width, since they are all degenerate. The bandlike distribution in Fig. 18 being an artifact of the plot.

The modes of the Stark ladder can be expressed as superpositions of compact modes, such as the fundamental one shown in Fig. 18. In addition to this mode, one can superpose two or more of them and create difractionless modes of different sizes (not shown). This fundamental compact mode is composed of three sites: two of them with given value A and one with value $-A$. All the rest of the ribbon sites are zero. This geometrical array prevents nearby sites from evolving, and thus difraction is completely arrested. Let us briefly comment on the stability properties of the fundamental stub mode. First, the mode is robust against noise on the initial amplitudes. This was also observed for the kagome and Lieb ribbons. The mode is also robust against the presence of anisotropic couplings, even for large anisotropy values. Finally, the mode is also robust against noise in the couplings. At large noise values, we observed some transfer of amplitudes among the three sites, producing a small oscillation of the participation ratio of the mode. The shape of the mode did not change though.

6. Nonlinear regime

As with the previous ribbons, the fundamental compact mode is also a nonlinear eigenstate. From Eq. (2), one obtains

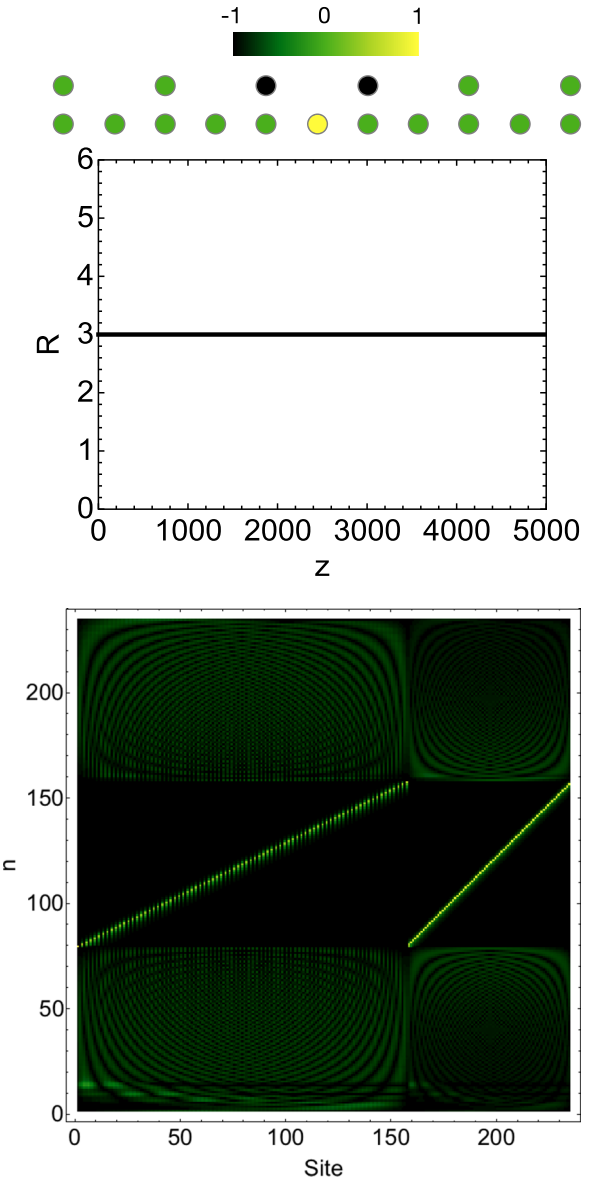

FIG. 18. Stub ribbon. Top: Evolution of the participation ratio of the fundamental stub compact mode, at long evolution distances. Inset shows the geometrical disposition of the fundamental compact mode. Bottom: Density plot of the eigenvectors of the stub ribbon, arranged in order of increasing eigenvalue.

after replacing the amplitudes and phases of the compact mode, a closed expression for the power curve

$$P = \frac{3}{\gamma}\Omega. \tag{8}$$

This relation is valid for any amount of power below and beyond the position of the bands. To be sure, at low powers the mode is unstable, becoming stable beyond a critical value of power (∼15.5). The shape of this compact mode does not change, as evidenced by the constant value of the participation ratio ($R = 3$). This nonlinear mode bifurcates from the flatband $\Omega = 0$, as Fig. 19 shows. On the other hand, for a nonlinear mode stemming from a single-site initial condition, the power curve (not shown) resembles the one

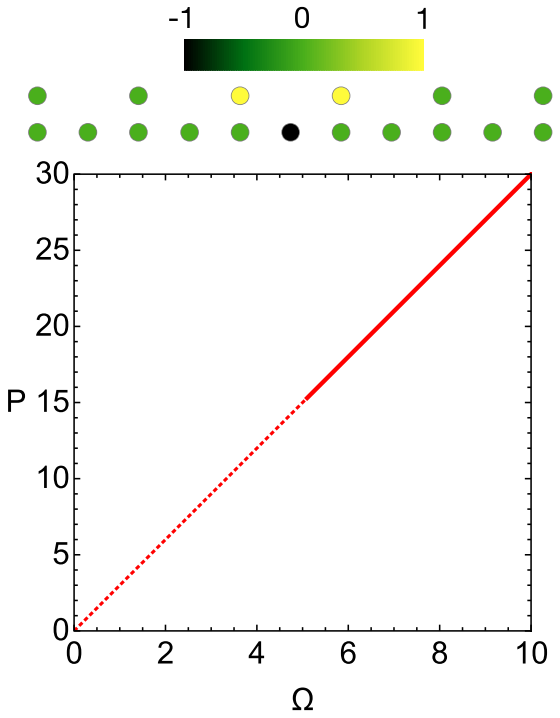

FIG. 19. Power P vs propagation constant Ω for the nonlinear fundamental mode for the stub ribbon. Solid (dashed) line denotes stable (unstable) portions.

for the Lieb ribbon, with little variations. In general for this case, the power curve is stable at large powers, and there is a minimum power for this nonlinear mode to exist. To the left of this critical propagation constant, the power raises but is linearly unstable.

III. CONCLUSIONS

We have examined the spectral characteristics of three quasi-one-dimensional lattices: the kagome, Lieb and stub thin ribbons. They are all characterized for having a flatband with degenerate eigenvectors that form a Stark ladder. These states can give rise to completely compact modes which do not diffract. This property is due to a precise geometrical combination of amplitude and phases that prevent the transfer of amplitude to nearby sites. Next, we focused on the simplest compact mode for each ribbon and examined its dynamical stability against noise in the initial conditions of the rings, anisotropy of the couplings, and random variations of the couplings. The results vary from ribbon to ribbon. In general for all three of them, it was found that they are stable against random changes in the initial values of the the ring sites. The stub and Lieb ribbons are stable against (nonrandom) anisotropies of the couplings, while the kagome ribbon is unstable. For randomness of the couplings both the Stub and Lieb systems are stable, while the kagome ribbon is unstable. When nonlinear effects are added to the picture, it was found that the fundamental compact mode of each ribbon *is also an eigenvector of the nonlinear eigenvalue problem*. In this case, the power versus propagation constant curve can be obtained in closed form. Moreover, this stationary nonlinear compact mode has a power curve that exists for all propagation constant values, even inside and across the linear bands. This is in marked contrast to the usual discrete soliton phenomenology, where a nonlinear mode can only exist outside the linear bands.

The robustness of the Lieb and stub ribbons give us hope that the goal of using flatband systems as possible candidates for stable robust long-distance image transmission systems could be at hand.

ACKNOWLEDGMENTS

This work was partially supported by FONDECYT grant 1120123, Programa ICM P10-030-F and Programa de Financiamiento Basal de CONICYT (FB0824/2008).

[1] A. Lagendijk, B. van Tiggelen, and D. S. Wiersma, Phys. Today **62**(8), 24 (2009).
[2] V. Apaja, M. Hyrkäs, and M. Manninen, Phys. Rev. A **82**, 041402(R) (2010).
[3] M. Hyrkäs, V. Apaja, and M. Manninen, Phys. Rev. A **87**, 023614 (2013).
[4] M. C. Rechtsman, J. M. Zeuner, A. Tünnermann, S. Nolte, M. Segev, and A. Szameit, Nat. Photon. **7**, 153 (2013).
[5] R. A. Vicencio, C. Cantillano, L. Morales-Inostroza, B. Real, C. Mejía-Cortés, S. Weimann, A. Szameit, and M. I. Molina, Phys. Rev. Lett. **114**, 245503 (2015).
[6] S. Mukherjee, A. Spracklen, D. Choudhury, N. Goldman, P. Öhberg, E. Andersson, and R. R. Thomson, Phys. Rev. Lett. **114**, 245504 (2015).
[7] C. L. Kane and E. J. Mele, Phys. Rev. Lett. **78**, 1932 (1997).
[8] F. Guinea, M. I. Katsnelson, and A. K. Geim, Nat. Phys. **6**, 30 (2010).
[9] A. Simon, Angew. Chem. **109**, 1873 (1997).
[10] S. Deng, A. Simon, and J. Köhler, Angew. Chem. **110**, 664 (1998).
[11] S. Deng, A. Simon, and J. Köhler, J. Solid State Chem. **176**, 412 (2003).
[12] M. Imada and M. Kohno, Phys. Rev. Lett. **84**, 143 (2000).
[13] E. Tang, J.-W. Mei, and X.-G. Wen, Phys. Rev. Lett. **106**, 236802 (2011).
[14] T. Neupert, L. Santos, C. Chamon, and C. Mudry, Phys. Rev. Lett. **106**, 236804 (2011).
[15] S. Yang, Z.-C. Gu, K. Sun, and S. Das Sarma, Phys. Rev. B **86**, 241112(R) (2012).
[16] T. Jacqmin, I. Carusotto, I. Sagnes, M. Abbarchi, D. D. Solnyshkov, G. Malpuech, E. Galopin, A. Lemaitre, J. Bloch, and A. Amo, Phys. Rev. Lett. **112**, 116402 (2014).
[17] F. Baboux, L. Ge, T. Jacqmin, M. Biondi, A. Lematre, L. Le Gratiet, I. Sagnes, S. Schmidt, H. E. Türeci, A. Amo, and J. Bloch, Phys. Rev. Lett. **116**, 066402 (2016).
[18] J. Mur-Petit and R. A. Molina, Phys. Rev. B **90**, 035434 (2014).

[19] K. Davies, K. Miura, N. Sugimoto, and K. Hirao, Opt. Lett. **21**, 1729 (1996).

[20] A. Szameit, F. Dreisov, H. Hartung, S. Nolte, A. Tunnermann, and F. Lederer, Appl. Phys. Lett. **90**, 241113 (2007).

[21] See, for instance, P. G. Kevrekidis, *The Discrete Nonlinear Schrödinger Equation: Mathematical Analysis, Numerical Computations and Physical Prespectives* (Springer, Berlin, 2009).

[22] See, for instance, Y. S. Kivshar and B. A. Malomed, Rev. Mod. Phys. **61**, 763 (1989); M. Johansson and Y. S. Kivshar, Phys. Rev. Lett. **82**, 85 (1999); A. R. Cowan and J. F. Young, Phys. Rev. E **68**, 046606 (2003); A. Khare, K. O. Rasmussen, M. R. Samuelsen, and A. Saxena, J. Phys. A **38**, 807 (2005); *ibid.* **42**, 085002 (2009); *ibid.* **43**, 375209 (2010).

[23] J. Schulenburg, A. Honecker, J. Schnack, J. Richter, and H.-J. Schmidt, Phys. Rev. Lett. **88**, 167207 (2002); O. Derzhko, J. Richter, A. Honecker, M. Maksymenko, and R. Moessner, Phys. Rev. B **81**, 014421 (2010).

[24] M. I. Molina, Phys. Lett. A **376**, 3458 (2012).